Unsteady Vortex Dynamics of Two-Dimensional Pitching Flat Plate Using Lagrangian Vortex Method

3 authors:

Duong Viet Dung
Vietnam National University, Hanoi

12 PUBLICATIONS   **10** CITATIONS

SEE PROFILE

Lavi Rizki Zuhal
Bandung Institute of Technology

48 PUBLICATIONS   **193** CITATIONS

SEE PROFILE

Hari Muhammad
Bandung Institute of Technology

30 PUBLICATIONS   **49** CITATIONS

SEE PROFILE

Some of the authors of this publication are also working on these related projects:

Project Vortex-wall interaction in viscous fluids View project

Project Vortex Interaction in a Viscous Fluid View project

Unsteady Vortex Dynamics of Two-Dimensional Pitching Flat Plate Using Lagrangian Vortex Method

Dung Viet Duong
School of Aerospace Engineering,University of Engineering and Technology,Vietnam National University, Ha Noi City, Vietnam
duongdv@vnu.edu.vn

Lavi Rizki Zuhal
Faculty of Mechanical and Aerospace Engineering,Institut Teknologi Bandung,Indonesia
lavirz@ae.itb.ac.id

Hari Muhammad
Faculty of Mechanical and Aerospace Engineering, Institut Teknologi Bandung, Indonesia
hari@ftmd.ac.id

ABSTRACT

Vortex dynamics of wakes generated by two-dimensional rectangular pitching flat plates in free stream are examined with direct numerical simulation using Lagrangian vortex method. The developed method simulates external flow around complex geometry by tracking local velocities and vorticities of particles, introduced within the fluid domain. The viscous effect is modeled using a core spreading method coupled with the splitting and merging spatial adaptation scheme. The particle's velocity is calculated using Biot-Savart formulation. To accelerate computation, Fast Multipole Method (FMM) is employed. The solver is validated by performing an impulsively started cylinder at Reynolds number 550. The results of the computation have reasonable agreement with references listed in literature. For the vortex dynamics of pitching flat plate, the detaching LEV creates a remarkable peak in the lift force before the end of motion for the different pitching cases. For the low Reynolds number, force generated by the pitching flat plate is fairly independent of Reynolds numbers. The current studies also observed that TEV produced at higher Reynolds number has a stronger suction than that at smaller Reynolds numbers.

CCS CONCEPTS

• **Particle-based Computational Fluid Dynamics**; • **Complex Flow Separation**;

KEYWORDS

Unsteady Laminar Separation, Vortex Particle Method, Vortex Identification Method

1 INTRODUCTION

Recently, the missions for micro-scaled aerial vehicles (MAVs) [1, 2] have been expanded from surveillance, environmental monitoring to communication. The MAVs are required to complete these missions in confined spaces, gusty and harsh environments. Therefore, the MAVs must have the ability to rapidly avoid obstacles. Accordingly, MAVs are designed to be small with maximum dimension less than 20 (cm) and weighing 100 (g). The proposed propulsion system for the MAVs is flapping motions of fixed wing of vehicles, which are working at high angle of attack (AoA) in order to enhance the performance of lift force.

Mechanisms of the lift enhancement depend significantly on the understanding of unsteady aerodynamics effect of wake development due to flow separation. It is well known as an unsteady dynamic stall. The MAVs are operated in the low Reynolds number range. Due to the effect of small Reynolds numbers, the phenomena of the dynamic stall is connected to formation of leading edge vortex (LEV) during the motions of the wing (translation, rotation and pitching).

Experimental and computational studies for the correlation between LEV and force enhancement have generally been conducted to include the effects of the rate of change of translational speed and angle of attack (AoA). This mechanism was investigated for low Reynolds number applications by Ellington et al. [3], who found that the attachment of a prominent bound vortex core to the leading edge of the upper wing could enhance lift force during the translational motion. The size of the LEV is proportional to the size of a low-pressure region over the top surface of the wing, which enhances the increased suction on the upper surface of the wing. Thus, the lift force is increased before the LEV detaches and advects downstream for three to four chord lengths of travel. Dickinson and Gotz [4] performed the aerodynamics force measurement of the flapping wing model, which is under impulsively started translation at high incidence angles of attack. They found that above 13.5^0, the LEV remains attached for the first two chord lengths of travel, which results in an 80% increase of lift compared to the performance measured five chord lengths later.

The work presented in this paper will provide insights on the evolving flow structure around 2D flat plate performing rapid maneuvers and its influence on the forces generated on the flat plate. Although the rapid maneuvers utilized by biological flyers such as birds and insects include complex motions with multiple degrees

of freedom, this study is limited to a set of canonical motions including pitching. The reasoning behind limiting the complexity of the motions for this study is to provide a better understanding on how the flow evolves for these simple motions and its effect on the aerodynamics forces. Results from the parametric studies of varying the frequency of flapping motions can provide insights for applied aerodynamicists towards designing flapping wing MAVs that are able to withstand the unsteady and three-dimensional effects of the flow on the maneuvering wings and body.

2 GOVERNING EQUATIONS

The vortex methods are based on the momentum equation and the continuity equation for incompressible flow which are written in vector form as follows:

$$\frac{\partial \underline{u}}{\partial t} + \left(\underline{u}.\nabla\right)\underline{u} = -\frac{1}{\rho}\nabla p + \nu\nabla^2\underline{u} \quad (1)$$

$$\nabla.\underline{u} = 0 \quad (2)$$

Taking the *curl* and *divergence* of equation 1) and simplify using (2) :

$$\frac{\partial \omega}{\partial t} + \left(\underline{u}.\nabla\right)\omega = \left(\omega.\nabla\right)\underline{u} + \nu\nabla^2\omega \quad (3)$$

$$\nabla^2 p = -\rho\nabla.\left(\underline{u}\nabla\underline{u}\right) \quad (4)$$

where $\underline{u}$ is velocity vector, p the pressure, and ρ the density. The vorticity ω is defined as

$$\omega = \nabla \times \underline{u} \quad (5)$$

This equation is solved numerically, by using a viscous splitting algorithm. The algorithm includes two steps. The first step, the so-called convection step, is to track particle elements, containing the certain value of vorticity, with their own local convective velocity by using Biot-Savart formulation

$$\underline{u}\left(\underline{x}, t\right) = \frac{1}{2\pi}\int\frac{\omega\left(\underline{x}', t\right) \times \left(\underline{x} - \underline{x}'\right)}{\left|\underline{x} - \underline{x}'\right|^3}d\underline{x}' \quad (6)$$

where $\underline{x}$ is the position vector. The term inside integral in Eq. 6) is integrated over all particles within the computational domain. The Biot-Savart relation is N-body problem that involves $O(N^2)$ evaluations. In order to overcome the N-body problem mentioned above, the Fast Multipole Method (FMM) is employed in this work to accelerate the velocity computation [5]. The method significantly reduces the velocity computation time due to the fact that interactions among particles are not computed directly. In viscous flows, the no-slip and no-through boundary conditions on solid surfaces must be satisfied. Employing the introduction of Nascent vortex element [6], the no-through and no-slip boundary conditions are satisfied. The detailed algorithms of this work are validated and employed by the work of Dung *et. al.* [7].
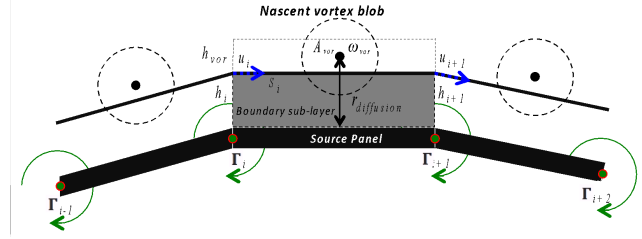
Figure 1: Production of Nascent Vortex Elements.

3 FAST MULTIPOLE METHOD

$O(N^2)$In order to overcome the N-body problem mentioned above, the Fast Multipole Method (FMM) is employed in this work to accelerate the velocity computation. The method significantly reduces the velocity computation time due to the fact that interactions among particles are not computed directly. In more details, the FMM, first, constructs the data of particles by tree structure of the box in which particles are laid on. Second, the direct interactions of box's centers are evaluated by using multipole expansions of all these centers. Finally, the interaction of all direct particle pairs is translated from these centers to their own particles. Therefore, it reduces amount of computation process to the order of $O(N)$.

4 NO-THROUGH BOUNDARY CONDITION

$O(N^2)$Bounded flow problems require the enforcement of the no-through condition on boundaries. Vortex element method is a mesh-free approach. Therefore, the enforcement of no-through boundary conditions is accomplished through the use of boundary element methods (BEM). The BEM calculates a vortex sheet's strength, which represents the slip velocity on the boundary necessary to satisfy no-through condition. In BEM, the boundary is discretized into panels and the vortex strength of each panel, Γ, is calculated. These vortex strengths or wall circulations represent initial vorticity vectors on the wall panels. The calculated vortex strength is a vector with two wall-tangent components and a normal component, which satisfied the no-through condition.

5 NO-SLIP BOUNDARY CONDITION

In viscous flows, the no-slip and no-through boundary conditions on solid surfaces must be satisfied. Due to the introduction of Nascent vortex element, the no-through and no-slip boundary conditions are satisfied. Figure 1 shows the sketch of the production of a Nascent Vortex Element. In Figure 1, S_i, h_i, u_i denote respectively length of an outer boundary element, vorticity layer thickness and tangential velocity at each node of the outer boundary. The sketch in the figure is used to show the process of satisfying the wall boundary conditions by diffusing vortex elements from the wall. The Nascent vortex element is convected and diffused by velocities: V_c and V_d, respectively. Once a Nascent vortex element is shed from the wall, a new vortex element, which satisfies the no-slip boundary condition above, is redistributed along the wall panel for the next time step.
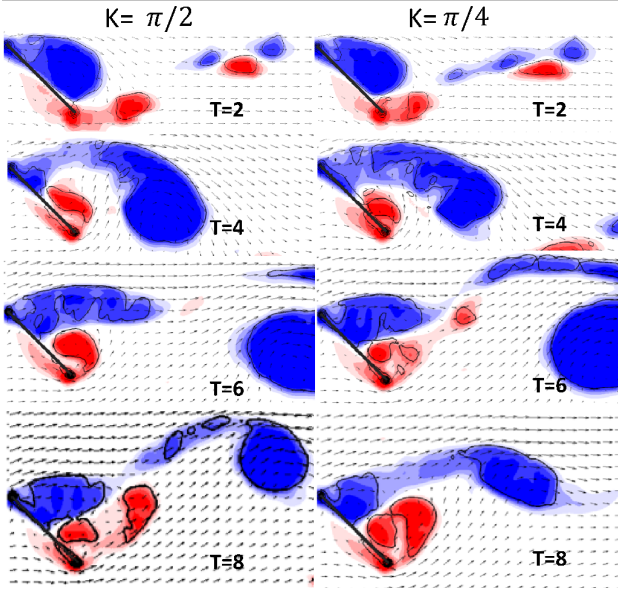
Figure 2: Contour of the Γ_2 function along with a single contour of the Q-criteria, showing the outline of vortex shedding behind the flat plate with two different reduced frequencies of pitching motions.

6 CORE SPREADING METHOD

In core spreading method, the core size magnitude is given by

$$\sigma(t) = \sqrt{4\nu\Delta t} \tag{7}$$

which represents the actual viscous diffusion. σ is the core radius of the vortex blob, and represents for the physical length scale of the vortex element. The rate of change of the core radius is

$$\frac{d\sigma_i}{dt} = \frac{2\nu}{\sigma_i} \tag{8}$$

Equation 8) manifests the diffusion. However, the total numerical truncation error, the so-called Lagrangian effect, increases proportionally with the spreading rate of change of particle core size. Increasing core size of each particle i makes the particle advect with its average velocity, rather than its local velocity. Hence, there is a need for a spatial adaptation scheme to control the core size of the particle to be small enough to minimize the Lagrangian effect and maintain the spatial resolution.

In this paper, we use the splitting scheme, to spatially adapt the flow field. In particular, if the core radius of the vortex blob is larger than a threshold, then the "parent" blob is split into the several smaller "children" blobs, and the vortex strength of the parent is distributed among the children. The children core radius is reset into the smaller core radius. Obviously, the children's cores are overlapped. Otherwise, the outstanding issue of the splitting scheme is to introduce the large amount of vortex elements. In other words, the number of vortex elements introduced is larger than the required vortex elements to sufficiently resolve the flow. Thus, the merging scheme is also proposed for the particle population control and for the overlapping control.
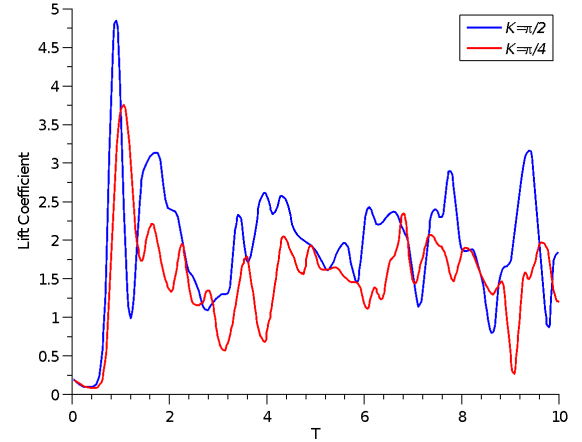
Figure 3: Time history of lift coefficient with different reduced frequencies of change rate of AoA at Re = 600.

7 ANALYSIS METHOD FOR VORTEX IDENTIFICATION

In order to record LEV there are many commonly used Eulerian vortex criteria, which identify coherent structures by an instantaneous local swirling motion in the velocity field, which are indicated by closed or spiral streamlines or pathlines in a suitable reference frame. There are a number of Eulerian methods being used in vortex identification. For example, Zhou *et al.* [8] developed the Q-criterion. Jeong and Hussain [9] developed the λ_2-criterion to identify pressure minima within 2D subspaces as a vortical structure. We employ two well-established Eulerian criteria for visualization of the relevant vortex structures: the Γ_1 and Γ_2 criteria of Graftieaux *et al.* [10], which has gained popularity due to its simplicity, and the Q-criterion by Hunt *et. al.* [11]. From each of these methods, we identify and track dynamically relevant points in the flow field that indicate the occurrence of physically significant phenomena.

8 TRACKING OF LEADING EDGE VORTEX OF A PITCHING FLAT PLATE

In this section, flat plate with rectangular planform with the length $D = 1$ undergoing a pitching maneuver in a constant freestream, $U_\infty = 1$ is considered. The Reynolds number is $Re = U_\infty D/\nu$, where ν is the kinematic viscosity. The Reynolds number for these studies is chosen to take into account issues of turbulence and to highlight the large-scale wake structures generated by the unsteady motion of the wing. In the present simulations, the $Re = 600, 3000$ are considered.

8.1 Configurations

The unsteady maneuvers considered in this work are defined by the function used by Eldredge et al. [12], for pitching motion. The function defines a smoothed linear rate of change of AoA, which allows for a continuous motion and avoids discontinuity in angular acceleration. The time history of the AoA of flat plate is given by
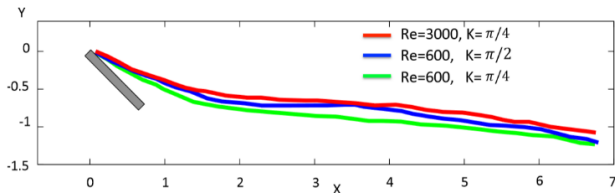
Figure 4: The temporal evolution of the spatial locations of the LEV with the two pitch rates and two Reynolds numbers.

Eq. 9).

$$\phi\left(t\right) = \frac{\Omega_0}{2a} log \left[\frac{coshcosh \ \left(a\left(t - t_1\right)\right)}{coshcosh \ \left(a\left(t - t_2\right)\right)} \right] + \frac{1}{2}\phi_0 \qquad (9)$$

In this equation, $t = D/U_\infty$ is the non-dimensional time, a controls the smoothing or acceleration, $\Omega_0 = \frac{U_\infty}{D}$ is the nominal rate of rotation. ϕ_0 is the maximum rotational angle in radians. The dimensionless quantities, t_1 and t_2 are start-up and end-up times of the unsmoothed motion, respectively in which $t_2 = t_1 + \phi_0 D/(2U_\infty K)$, where K is the reduced frequency. In this paper ϕ_0, t_1, a are set to be $\pi/4$, 1 and 5.2 while the effect of parameter K on the lift generation is studied by setting two values: $\pi/2$ and $\pi/4$.

8.2 Results and Discussions

Figure 2 shows the instantaneous contours of the Γ_2 function along with a single contour of the Q-criteria, showing the outline of vortex shedding behind the flatplate with two different reduced frequencies of pitching motions. The contour of Γ_2 function is colored from -0.9 to 0.9. The figure shows that the detachment of LEV in the case of smaller reduced frequency $K = \pi/4$ is slightly delayed in time compared with the case of $K = \pi/2$, even though the size of LEVs in both cases are similar. The only obvious difference of two cases is the trailing edge vortex, which affects the formation and detachment process of the LEV.

Figure 3 shows the time history of lift coefficient for the flat plate undergoing the pitching motions with different reduced frequencies of rate of change of AoA at Re = 600. For all pitch rates considered, there is a peak in C_L due to the angular acceleration of the wing. The amplitude of the peak is related to the smoothing value a in Eq. 7). For both the $K = \frac{\pi}{2}, \frac{\pi}{4}$ reduced frequencies, the maximum lift are achieved at about $t = 1$ and 1.2, respectively. The maximum lift being achieved before the end of the pitching motion is due to the formation and detachment of the LEV, which provides the enhanced lift. For both cases, as the plate continues to pitch, C_L begins to increase to a maximum value for all pitch rates considered. This increase in C_L is attributed to suction from the LEV. As the pitch rate is decreased, we notice a gradual reduction in the slope of the lift curve from the time $T = 2$.

Figure 5 presents contour of the Γ_2 function along with a single contour of the Q-criteria, showing effect of Reynolds numbers on the LEV and vortex shedding. The results are presented in an inertial reference frame at $T = 2$, 4 with two Reynolds numbers $Re = 600$, 3000, respectively.

The temporal evolution of the spatial locations of the center of LEV with the two pitch rates and two Reynolds numbers (600, 3000) are depicted in Figure 4. We note that the calculation of the LEV
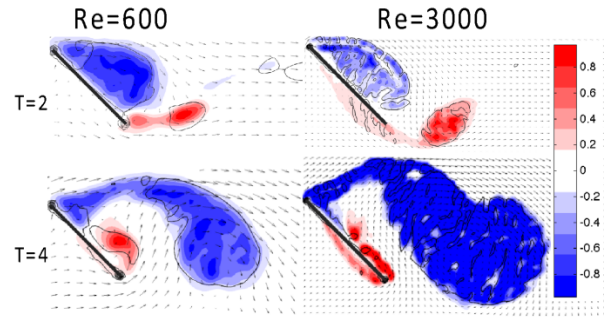
Figure 5: Contour of the Γ_2 function along with a single contour of the Q-criteria, showing effect of Reynolds numbers on the LEV and vortex shedding.
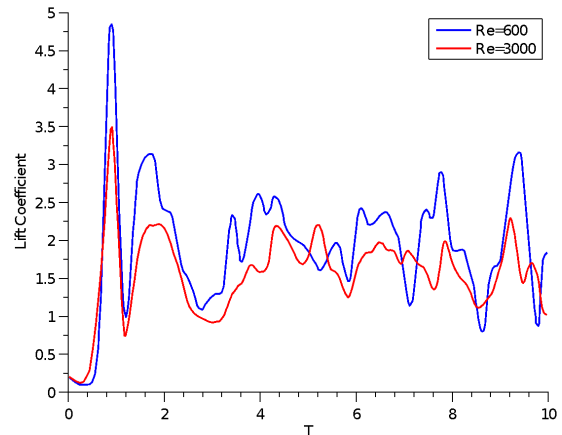
Figure 6: Time history of lift coefficients with different Reynolds numbers.

centers begins at different times for the two different pitch rates, due to the time it takes for the LEV to initially form. Also, while the maximum theoretical value for the center of the vortex is $\Gamma_1 = 1$, we selected a threshold of $\Gamma_1 > 0.95$ for the calculation and then select the maximum value of Γ_1 as the center of the vortex. For the two different reduced frequencies ($K = \frac{\pi}{4}, \frac{\pi}{2}$), the LEV centers travel from the leading edge in roughly the same direction, until it advects almost one chord length downstream. Also, it can be observed that as the Reynolds numbers increase, the trajectory of LEV centers does not deviate significantly from each other.

As the figure shown, the similar features of formation of LEV and the shedding process are clearly observed, namely the shedding of the starting vortex from the trailing edge, the development of the tip vortices, and the initial roll up of the vortex sheet from the leading edge forming the LEV. The only obvious difference between the two flow fields is the strength of the trailing edge vortex. The TEV at higher Reynolds number has a stronger suction than smaller Reynolds numbers. The lift coefficient, shown in Figure 6, also agrees with the observation of similar formation and shedding processes of LEV for the two different Re cases mentioned above.

9 CONCLUSIONS

Two-dimensional direct numerical simulations via the Lagrangian vortex method have been performed to examine the vortex dynamics for impulsively started cylinders at Re =550 and pitching flat plates at a range of pitch rates. In addition, the vortex dynamics in two cases have been studied using a range of identification and tracking techniques. Eulerian vortex core identification methods such as Γ_1, Γ_2 and Q recorded the location of the LEV instantaneously. In particular, the recorded vortex core moves downstream at a relatively constant speed. Meanwhile, the LEV vortex advects downstream after shedding while the attached TEV vortex is still growing.

For impulsively started cylinder cases, for low Reynolds number cases (600 and 3000), the results were validated to be convergent and in good agreement with references in terms of the wake structures and streamwise centerline velocity. For the case of pitching flat plate, the detaching LEV creates a peak in the lift force before the end of motion for the different pitching cases. In addition, the effect of Reynolds numbers was studied. The results show that for the low Reynolds number considered in this work, that force generated by the pitching flat plate is fairly independent of Reynolds numbers. The current studies also observed that TEV produced at higher Reynolds number has a stronger suction than that at smaller Reynolds numbers.

ACKNOWLEDGMENTS

REFERENCES

[1] P. G. Ifjuand, A. D. Jenkins, S. Ettingers, Y. Lian, W. Shyy, AIAA, (2002)
[2] K. D. Jones, F. M. Platzer, AIAA, 37 (2006)
[3] C. Ellington, Journal of Experimental Biology, 202 (1999)
[4] M. H. Dickinson, K. G. Gotz, Journal of Experimental Biology, 174 (1993)
[5] L. Greengard, V. Rokhlin, Journal of Computational Physics, 73 (1978)
[6] K. Kamemoto, Brazilian C. T. Sciences and Engineering, 26 (2005)
[7] D. V. Dung, L. R. Zuhal, H. Muhammad, Journal of Mechanical Engineering, 12 (2015)
[8] J. Zhou, R. J. Adrian, S. Balachandar, T. Kendall, J. F. M., 387 (1999)
[9] J. Jeong and F. Hussain, Journal of Fluid Mechanics, 285 (1995)
[10] L. Graftieaux, M. Michard, N. Grosjean, M. S. T., 12 (2001)
[11] J. C. R. Hunt, A. Wray, P. Moin, Center for turbulence research report, (1988)
[12] J. D. Eldredge, Journal of Computational Physics, 221 (2007)